

Contents

Table of Contents	i
List of Figures	i
List of Tables	ii
1 Coupling of Nanodiamonds to Photonic Structures	1
1.1 Additional Experimental Methods	2
1.1.1 Nanomanipulator	2
1.1.2 Determination of The Position of Nanodiamonds	3
1.1.3 The Pick-And-Place Process	5
1.2 Coupling SiV centers to Vertical-Cavity Surface Emitting Lasers	7
1.2.1 Vertical-Cavity Surface Emitting Lasers	7
1.2.2 SiV center in a Vertical-Cavity Surface Emitting Laser	9
1.3 Antennas	13
1.3.1 Plasmonic Antennas	16
1.3.2 Structure of the Plasmonic Antennas	18
1.3.3 SiV center in a Plasmonic Double Bowtie Antenna	19
Index	22

List of Figures

1.1	Nanomanipulator in a SEM setup	3
1.2	Detail of nanomanipulator tips	4
1.3	Cross markers assisting identification of nanodiamonds	4
1.4	Combining fluorescence light and laser scanning microscope to identify nanodiamonds	5
1.5	Sketch of the pick-and-place process	6
1.6	Nanomanipulator carrying a nanodiamond	7
1.7	Sketch of a vertical-cavity surface emitting laser	8
1.8	SEM image of an array of VCSELs	9
1.9	Emission spectra and optical power of VCSEL Bm4	10
1.10	Scans of VCSELs with and without SiV center	11
1.11	SiV center properties before and after pick-and-place	11
1.12	Comparison of intensities between VCSEL Bm4 and VCSEL Bm2	12
1.13	Comparison of spectra between VCSEL Bm4 and VCSEL Bm2	13
1.14	Reflectivity of VCSEL Bm4	14
1.15	(a) Picture recorded with a commercial high resolution laser scanning microscope. The area shaded in blue represents the photoluminescence scan in image (b). (b) Photoluminescence scan of a $8 \mu\text{m} \times 13 \mu\text{m}$	14
1.16	<caption>	15
1.17	Image of the sample surface of 100 nm wet-milled nanodiamonds spin-coated on an iridium substrate illuminated with diffuse white light. The white bars are the horizontal bars of the cross markers which serve as a coarse orientation on the sample surface, the white dots are nanodiamonds, the big black spot is an artifact.	15
1.18	16
1.19	<caption>	18
1.20	18
1.21	<caption>	19
1.22	<caption>	21
1.23	<caption>	21
1.24	<caption>	21
1.25	<caption>	22
1.26	<caption>	22
1.27	<caption>	23

List of Tables

Chapter 1

Coupling of Nanodiamonds to Photonic Structures

In the previous chapter, we reported on photoluminescence properties of different sets of SiV centers. Across the available samples, emitters were found to exhibit considerable variations in wavelength, linewidth as well as intensity of zero-phonon-lines. This broad variety in combination with the ability to examine SiV centers individually opens up the possibility to preselect emitters according to certain desired parameters. These are spectroscopic as well as technical in nature. The former include parameters such as narrow linewidth, high countrates and single photon emission. The latter includes the density of SiV centers on the substrate surface as well as the actual size of the nanodiamonds hosting SiV centers.

Once suitable emitters are identified, their host nanodiamonds can be moved with precision using pick-and-place methods. In particular, SiV centers may be transferred and coupled to photonic structures where their extraordinary properties can be exploited to create single photon source. Such sources are useful tools, widely required for applications in metrology and various quantum technologies such as quantum computing or quantum cryptography.

In the scope of this thesis, nanodiamonds including suitable SiV centers were identified and coupled to two different kinds of structures: Vertical-Cavity Surface Emitting Lasers (VCSELs) and plasmonic nanoantennas.

To create a hybrid-integrated single photon source, a nanodiamond containing an SiV center placed onto a VCSELs. The SiV center is positioned such that it is directly pumped by the VCSEL output laser beam. Thus, the emission of the SiV center is steered indirectly via the operation of the VCSEL. Through the use of suitable optical filters allowing only SiV center fluorescence light to emerge, a controlled single photon source can be realized in principle. This system is interesting in the context of metrological applications, as it constitutes a promising building block for a portable device ready to calibrate single photon detectors.

Coupling SiV centers to plasmonic nanoantennas aims at enhancing the detectable photoluminescence intensity of an emitter. Obtaining a single photon source with a photon flux rate large enough to reliably and precisely be measured by a low photon flux detector is a key requirement for applications in metrology [?].

1.1 Additional Experimental Methods

Coupling SiV centers to photonic structures requires specialized experimental methods. The major challenge consists of transferring a single nanodiamond hosting an SiV center precisely at a specified position within a given photonic structure. Since the SiV center is to function as the photoluminescence emitter, it must not be damaged during the relocation process.

In the context of this thesis we explored the following methods to couple nanodiamonds to photonic structures:

1. Directly spin-coat the target structures with a nanodiamond solution and consecutively look for a structure containing a nanodiamond with an SiV center exhibiting the desired spectroscopic properties. Frankly, this method relies on chance and is only feasible for the application with antenna structures due to the large number of antennas on one substrate. It is not advised to be used with VCSELs because of their morphology and the small number of VCSELs on an individual piece of substrate.
2. Identify nanodiamonds containing suitable SiV centers and individually relocate them to the destination structure using the tip in a scanning electron microscopy to perform a pick-and-place routine. For this method to be effective, nanodiamonds must have a certain size. The obvious advantage of this method is the fact that only the very best emitters are used. Furthermore, the pick-and-place process can be monitored in realtime. On the other hand, the electron radiation present during the pick-and-place process may damage the SiV center, introducing a risk of completely invalidating an emitter.
3. Identify nanodiamonds containing suitable SiV centers and individually relocate them to the destination structure using an atomic force microscope to perform a pick-and-place routine. While this method has the advantage that the nanodiamonds are not irradiated with electrons, the disadvantage is that it is not possible to observe the picking process in real time. As a consequence, the area of the preselected nanodiamond has to be scanned after every pick-up attempt, which is prohibitively time consuming and therefore was not further pursued after initial trials.

In the following we detail the pick-and-place technique since it is the key technique in this chapter. We also discuss the properties of the nanomanipulator and how we identify nanodiamonds suitable for pick-and-place transfer. The pick-and-place process itself is very fickle and difficult to execute correctly. We are grateful for the guidance and support provided by C. Pauly, group of F. Mücklich, Saarland University in addition to the nanomanipulator setup itself.

1.1.1 Nanomanipulator

The nanomanipulator used for our experiments (Kleindiek, model MM3A-EM) has a exchangeable tungsten tip mounted inside a Thermo Scientific™ Helios NanoLab™ DualBeam™ microscope. This device combines a focussed ion beam and an electron microscope. The bent nanomanipulator tip can be seen in Figure ?? has 3 degrees of freedom: up/down and left/right both in an arc up to 240°, and 12 mm in/out.

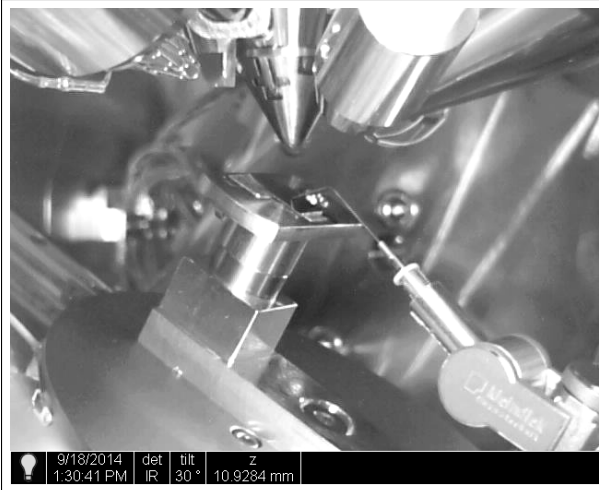


Figure 1.1: Image of the nanomanipulator mounted in the FIB. The arrows indicate the degrees of freedom of motion of the nanomanipulator. The custom made workbench is situated in the middle of the picture. On top of it, there is a 1 cm^2 substrate with coated nanodiamonds, the nanomanipulator tip pointing to the middle of it. Behind it, there is the target vertical-cavity surface emitting laser. Perpendicular to the workbench, the objective of the electron microscope can be seen. The angled cone perpendicular to the top edge of the image is the objective of the focussed ion beam.

Before using the nanomanipulator, its tip was “sharpened” with a focussed ion beam by etching away tungsten with gallium ions. Its final radius of curvature amounts to 100 nm. The sharpening enables the pick-up of nanodiamonds of a size suitable for use with photonic structures. In Figure 1.2a two sharpened tips are shown.

1.1.2 Determination of The Position of Nanodiamonds

Using the confocal setup detailed in ?? we identified nanodiamonds containing SiV centers suitable for the use in photonic structures. However, to actually move those nanodiamonds to a target photonic structure the SEM setup described in the previous section must be used. This implies that after substrates containing suitable nanodiamonds are mounted in the SEM setup, the same nanodiamonds must be located on the substrate in order for the nanomanipulator to address them correctly. To facilitate this and help locate relevant nanodiamonds, $10\text{ }\mu\text{m}^2$ cross markers with a nominal depth of 40 nm were milled into the iridium coating of the silicon substrate using the focussed ion beam prior to spin-coating the substrate with nanodiamond solution. The markers were arranged in a regular 11×11 grid covering an area of $0.5\text{ mm} \times 0.5\text{ mm}$. Figure 1.3a illustrates a sample array. Typically three arrays of markers were milled per substrate used.

To record the position of a nanodiamond with respect to a cross marker, we used two different methods:

In the first method the confocal setup is used with a white light source illuminates the sample from the side at an acute angle. As a result, the edges of the cross markers become visible in the fluorescence light scan, see Figure 1.3b. After turning the white light lamp off, the

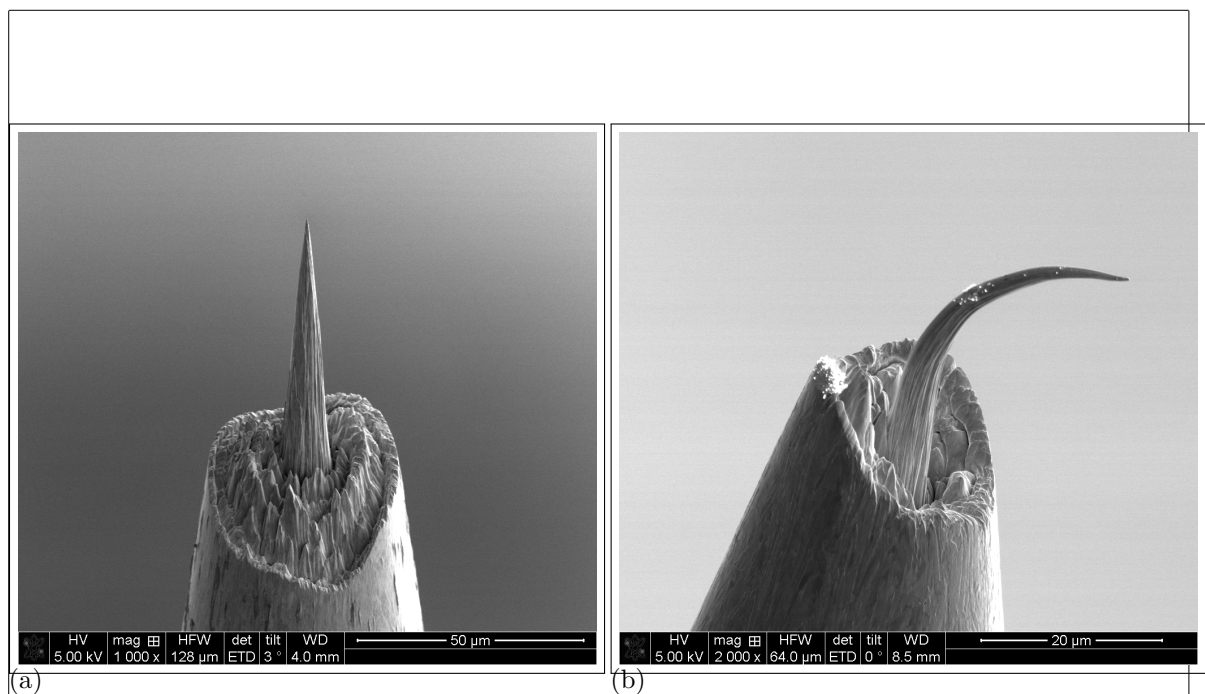


Figure 1.2: Detail of tips used as nanomanipulators. The actual tip can be seen projecting out from a bigger supporting structure. (a) Well-formed tip after sharpening. (b) Bend tip, silently attesting to the use of excessive force.

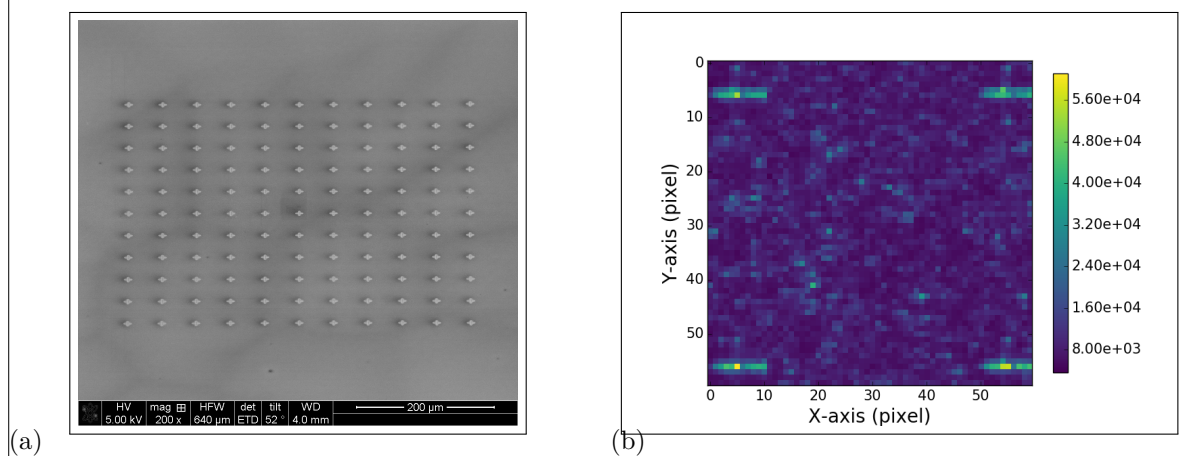


Figure 1.3: (a) Top-view of a regular array of cross markers. (b) White light scan of an area. Cross markers can be seen in all four corners.

same area is scanned again to record the fluorescence from the SiV centers. An overlay of the two images identifies the position of fluorescent SiV centers with respect to the cross markers. The disadvantage of this method is the increased time consumption, as every scan for every subregion of the sample has to be performed twice. As only fluorescence light scans are performed, no information about the size of individual nanodiamonds is available. Furthermore, it remains unknown whether nanodiamonds are present in isolation or close to each other. Such information is only available in the SEM where the pick-and-place is conducted. It is only at this later stage, that individual nanodiamonds can be excluded as unusable for the pick-and-place process. For such nanodiamonds the time spend of characterizing its properties was unfortunately wasted.

To mitigate this problem, a more efficient method consists of scanning the substrate first using a commercial laser scanning microscope. The laser scanning microscope is a confocal microscope where the focus of a laser can be used to obtain the height of a structure. When scanning an array of cross markers a greyscale image is obtained, where the grey value corresponds to the height deviation of a structure. As a result, both the crosses with a nominal depth of 40 nm and the nanodiamonds themselves are revealed as darker shades of grey. In contrast to the previous method, information on the size and isolation of nanodiamonds is accessible. After scanning the substrate with the laser scanning microscope, it is inserted into the confocal setup. While observing the surface with a CCD camera, a specific cross marker is chosen as the starting point for a fluorescence light scan. Comparing the laser scanning microscope image and a fluorescence light scan, fluorescent dots of the fluorescence light scan can be attributed to nanodiamonds in the laser scanning microscope scan. ?? illustrate the process.

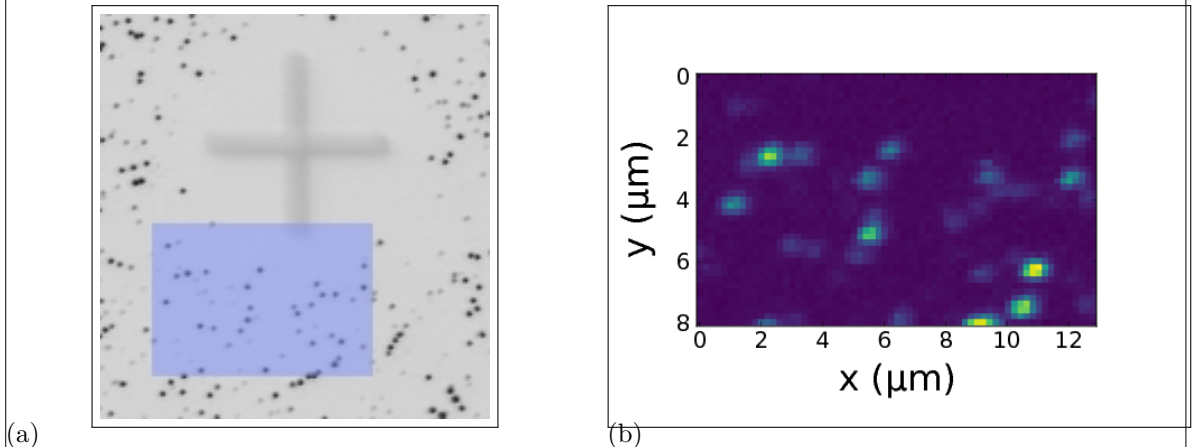


Figure 1.4: a) Picture recorded with a commercial high resolution laser scanning microscope. Cross marker is visible as well. b) Photoluminescence scan of a $8 \mu\text{m} \times 13 \mu\text{m}$ corresponding to the blue shaded area in b). The area shaded in blue represents the photoluminescence scan in image b).

1.1.3 The Pick-And-Place Process

The pick-and-place process aims to transfer a select nanodiamond between two substrates using the tip mounted inside a scanning electron microscopy. The advantage of using the

SEM tip as a nanomanipulator lies in the fact that the progress of the manipulation process can be visualized directly, allowing for a better control of the operation. Figure 1.5 illustrates the process.

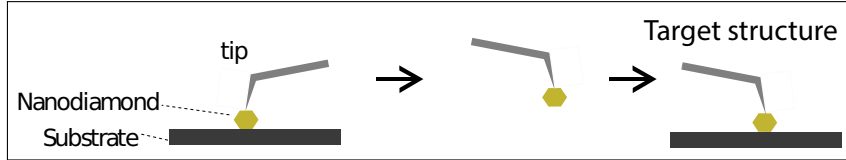


Figure 1.5: Sketch of the pick-and-place process

After we identified nanodiamonds as well-suited for transfer to the target structure, both the substrate with the nanodiamonds and the target structure were mounted inside the SEM. The process was performed using a high resolution mode with a low acceleration voltage of the SEM of 1 keV and a current of 1.7 nA. The tip is approaching the target pre-selected nanodiamond from above. As the SEM objective is mounted above the nanomanipulator, the proximity the nanomanipulator tip to the nanodiamond is not observable. To enable the tip of the nanomanipulator to pick up a target nanodiamond a precise approach is necessary. To facilitate this difficult procedure, the approach is divided into two stages: A coarse stage and a fine stage.

In the coarse stage the distance between tip and target nanodiamond is indirectly estimated from the shadow the tip itself casts onto the substrate and the focus area. As the tip approaches the target, the shadow of the tip starts to coincide with the nanodiamond position. At this point the fine stage of the approach begins in order to cover the remaining distance. To precisely control the final approach the focus of the SEM is used. Note that, as the distance between the tip and the target decreases, the focus must become sharp. Note that if the SEM is focused on the nanodiamond, the tip is out of focus and appears blurry. However, as the distance between the tip and the target decreases, the focus must become sharp. Thus the tip must be moved with utmost care until the focus becomes sharp at which point the tip touches the nanodiamond and pick-up can commence. While the process appears straightforward in concept, it is extremely challenging to operate the involved machinery to the required precision. As can be seen in Figure 1.2b it is easy to overshoot the target and to ruin the tip in the process.

When performed correctly, the nanodiamond sticks to the tip due to adhesion when the both get in contact, see Figure 1.6a. The nanomanipulator is then moved to the target structure and the approach procedure is applied in reverse. Figure 1.6b illustrates the tip of the nanomanipulator carrying a nanodiamond towards its destination structure. Depending on the material of the target structure, the nanodiamond either sticks to the structure right away due to higher adhesion forces between the nanodiamond and the structure (as is the case for golden plasmonic antennas). Alternatively, a sideways motion of the nanomanipulator tip must be used in an attempt to strike-off the nanodiamond. Either way, with patience it is possible to place a nanodiamond in a target position within a precision of a few nanometers.

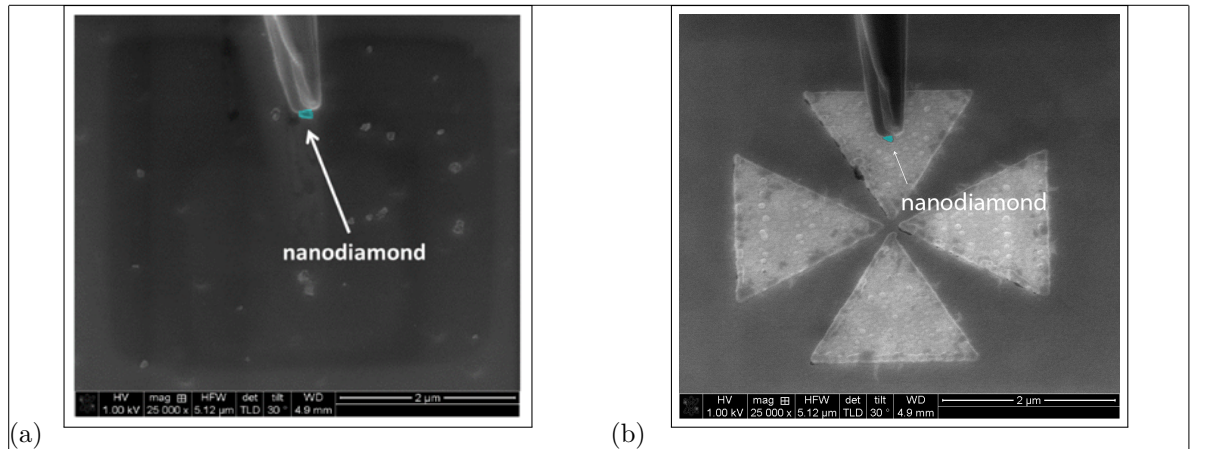


Figure 1.6: a) Tip of the nanomanipulator after successful pick-up of a nanodiamond. b) Tip of the loaded nanomanipulator approaching the target structure about to deliver a nanodiamond.

1.2 Coupling SiV centers to Vertical-Cavity Surface Emitting Lasers

In the context of metrology, controllable single photon sources, operating at room temperature, are an extremely important prospect. Such devices are anticipated to play a key role in the development and calibration of detectors and measurement methods aiming to resolve optical flux down to single-photon resolution [?]. As such single photon source form a cornerstone of the efforts directed towards the redefinition of the candela in terms of single photons, see discussion in ??.

Here we attempt to create a hybrid-integrated single photon source by placing a nanodiamond ideally containing a solitary SiV centers onto a vertical-cavity surface emitting lasers (VCSELs). The SiV center is situated such that output laser of the VCSEL can be used to optically excite the color center. Since the VCSEL laser can be controlled very well, SiV center operation can be steered reliably. Through the use of suitable optical filters allowing only SiV center fluorescence light to emerge, a controlled single photon source can be realized in principle.

In the following we give a short discussion of VCSELs. Next we discuss the coupling of SiV centers to VCSELs and report on the optical properties of the resulting hybrid-integrated light source.

1.2.1 Vertical-Cavity Surface Emitting Lasers

A vertical-cavity surface emitting laser is a type of semi-conductor laser diode [?, ?, ?]. Figure 1.7 illustrates a common design consisting of a *p*-layer on top and a *n*-layer at the bottom separated by a so-called active area. When a current is applied across the device, charge carriers migrate towards the active region. Holes act as charge carriers in the *p* region, whilst electrons carry charge in the *n*-region. The material properties of the active region is chosen such that when electrons and holes spontaneously recombine, a photon is emitted in the process. Electron-hole pairs can also dissipate via the creation of phonons leading to losses

in the form of heat. To define the region for recombination to occur and to control the optical properties of the device, additional thin layers of semiconducting material can be introduced in the active area. These result in the formation of quantum wells with associated energy levels and resulting preferred transitions with well-defined energies for the recombination of electrons and holes.

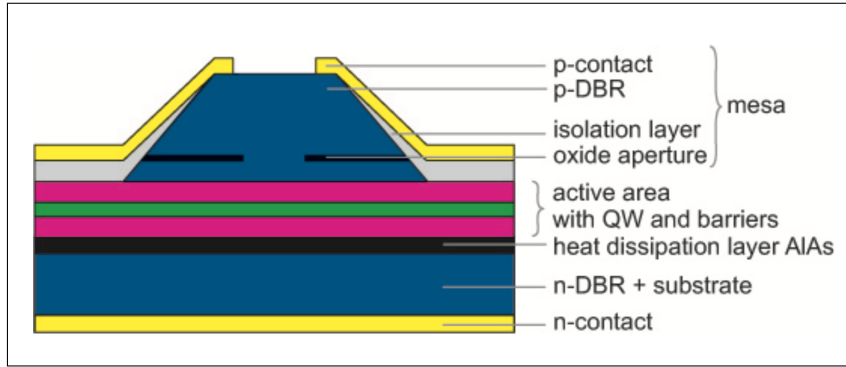


Figure 1.7: Illustration of a VCSEL laser diode [?]. When a current is applied across the device via contacts (yellow), holes and electrons migrate from the *p*-region (blue, top) and the *n*-region (blue, bottom) towards the active region (purple+green, center) where they recombine emitting photons. A quantum well is inserted in the active region, shaping the recombination process. *p*-region and *n*-region are acting as DBRs forming the resonator of the laser diode. When enough photons are gained by via stimulated emission, a laser beam emerges from the *p*-region after passing an oxide aperture.

To achieve lasing, stimulated recombination and thus stimulated emission of photons is required. To facilitate this both *p*-region and *n*-region are constructed in a layered fashion allowing them to act as highly-efficient distributed Bragg reflectors (DBR). Thus the active region is sandwiched by two mirrors forming the resonator of the laser diode. Spontaneously emitted photons thus are temporarily trapped continuously interacting with the active region. Provided the presence of sufficient electron-hole pairs, a photon can stimulate their recombination and thus the emission of further identical photons which themselves increase the stimulated emission. If enough identical photons are gained in this process, a coherent laser beam is formed by the fraction of photons escaping the resonator through the *p*-region. As a result the laser beam produced by a VCSEL is perpendicular to the substrate it resided on.

VCSELs have a range of properties that make them particularly interesting for industrial applications such low power consumption, ease of fabrication and cheap production. As a result, VCSELs are utilized in a broad range of applications including fiber optic communications or precision sensing and are used widely in commonly encountered devices such as computer mice or laser printers [?].

In the context of this thesis VCSELs offer several advantages. Their output beam is perpendicular to the substrate surface and suitable to excite SiV centers. This means that nanodiamonds containing SiV centers can simply be placed onto the device. Furthermore their physical size is ideal for the nanodiamonds we work with. The small size of VCSELs will make it easier to deploy the resulting hybrid-integrated light sources in future applications.

1.2.2 SiV center in a Vertical-Cavity Surface Emitting Laser

To conduct our research, we received an array of red AlGaInP-based oxide-confined VCSELs from P. Michler, Stuttgart University. The array includes three individually operable VCSELs, two of which, labeled VCSEL Bm4 and VCSEL Bm2 were used in our experiments, see Figure 1.8a.

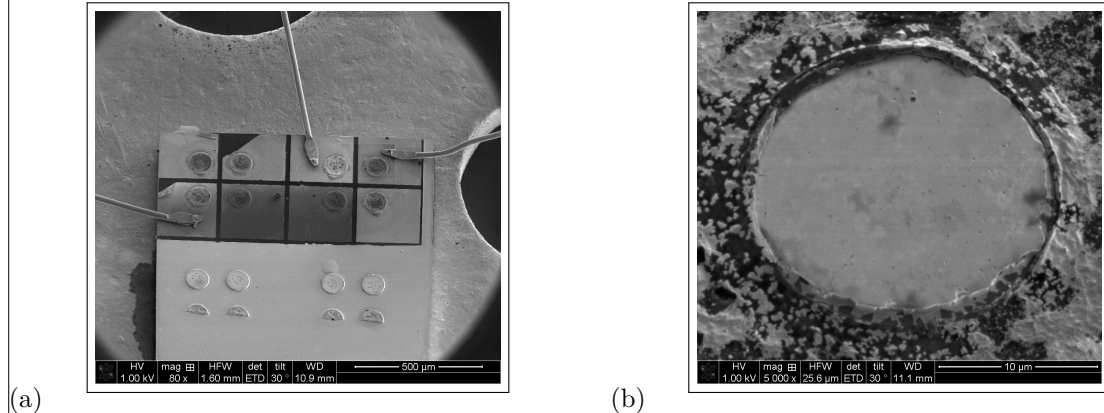


Figure 1.8: (a) SEM image of an array of VCSELs. The three wires are the anodes, which are connected to the top layer (*p*-contact) of the VCSEL. Therefore, three of the VCSEL structures can be operated. VCSEL Bm4 is located in the top right while VCSEL Bm2 to the left of it. (b) Detail SEM image of the top of VCSEL Bm4. The circular middle part is the hole in the *p*-contact through which the top DBR is visible. The smaller active diameter measures $5.8 \mu\text{m}$ through which the laser light exits the structure is not visible in the SEM. A successful pick-and-place operation positions a nanodiamond hosting an SiV center directly in the path of the VCSELs laser.

The VCSELs we obtained use a *n*-type DBR consisting of 50 pairs of AlAs/Al_{0.5}Ga_{0.5}As mirror pairs while the *p*-type DBR is formed by 36 Al_{0.95}Ga_{0.05}As/Al_{0.5}Ga_{0.5}As [?]. The active region itself consists of 4 GaInP quantum wells. An oxide aperture in a field node of the standing wave serves as a spatial filter for maximum modal gain by confining the current and the optical mode. The active diameter which is defined by the oxide aperture is $5.8 \mu\text{m}$.

The available VCSELs are perfect candidates for the excitation of SiV centers in a hybrid integrated single photon source for several reasons. They exhibit a circular beam profile, have low divergence angle and emit linearly polarized light. Their physical size and the fact, that their output beam is perpendicular to the substrate implies that our nanodiamonds containing nanodiamonds can simply be placed onto the structure light-emitting region using pick-and-place methods, see Figure 1.8b. Thus the VCSELs output laser can be used to optically excite SiV centers.

As a first step towards using VCSELs to excite color centers, we characterized the behaviour of VCSEL Bm4. To this end we operated it at currents of 1.5 mA and 3 mA and recorded the resulting lasing wavelength. The emission spectra showed that the emitted continuous wave laser light to be around 655 nm in wavelength for both currents, see Figure 1.9a. Previous research within the authors group recorded SiV center intensity maxima at excitation wavelengths of 720 nm and 680 nm [?], aligning reasonably well with the output wavelength of VCSEL Bm4.

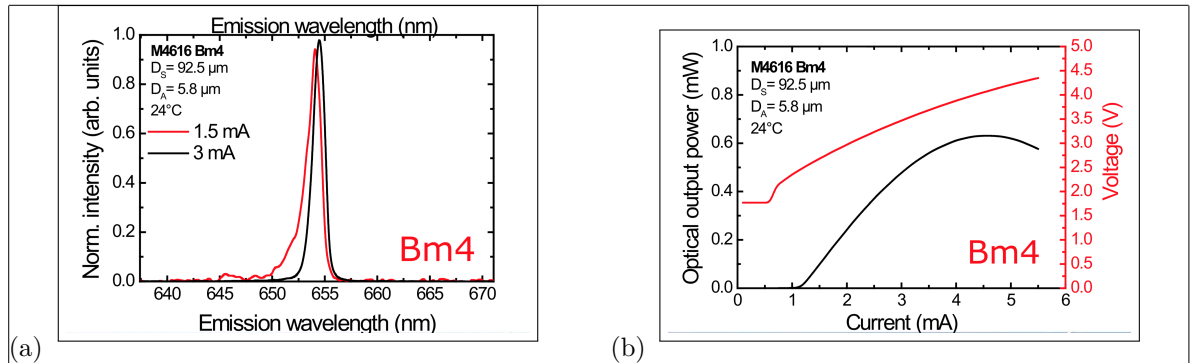


Figure 1.9: (a) Emission spectrum of VCSEL Bm4 at two different currents. (b) Optical output power and voltage of VCSEL Bm4 in dependence of input current. \square

The optical output power of VCSEL Bm4 as a function of the current applied is given in Figure 1.9b. In addition, the resulting voltages are shown. It can be seen that the maximum power of $\approx 0.6 \text{ mW}$ is reached for moderate currents of $\approx 4.5 \text{ mA}$. While the available optical powers are small comparable to using a conventional laser, low powers are sufficient for initial explorations.

The next step consists of selecting a suitable nanodiamond containing an SiV center followed by transferring it onto of VCSEL Bm4. To this end nanodiamonds 200 nm in size were grown with the CVD method in an iridium coated silicon wafer. We refer the reader to ?? for details on the process.

Next, using the confocal setup described in ?? a nanodiamond was identified exhibiting one dominant line at 746.0 nm with a linewidth of 1.9 nm. Its position on the substrate was determined consecutively using a white light laser scan as described in subsection 1.1.2. Given the position of the nanodiamond it was then transferred to VCSEL Bm4 and placed precisely in its active, i.e. light-emitting region. The process of introducing an SiV center to another structure is referred to as coupling.

After successful transfer VCSEL Bm4 was inserted into the confocal setup. Using the laser from the confocal setup we checked if the pick-and-place process caused any modification of the spectroscopic properties of the SiV center such as a decrease of countrate or a modification of the fluorescence light spectrum. During these checks, the VCSEL itself was not active.

As a first check, we scanned the VCSEL surface in an attempt to detect the activity of the introduced SiV center. Figure 1.10a shows the SiV center as a bright dot in the aperture of VCSEL Bm4. For comparison, a Vertical-Cavity Surface Emitting Laser without coupled SiV center exhibits solely background counts which is shown in Figure 1.10b.

The spectrum of the SiV center in the transferred nanodiamond was investigated before and after the pick-and-place process. section 1.11 shows that the original spectrum before nanodiamond transfer exhibits one dominant line at 746.0 nm, denoted line A. Furthermore, two minor peaks can be seen. The lower wavelength peak is denoted as line B. Interestingly, after the pick-and-place process, a different picture emerges shown in section 1.11. The once dominant line A is strongly reduced. The new dominant feature is line B. Note that the count rate of line B remained the same before and after pick-and-place.

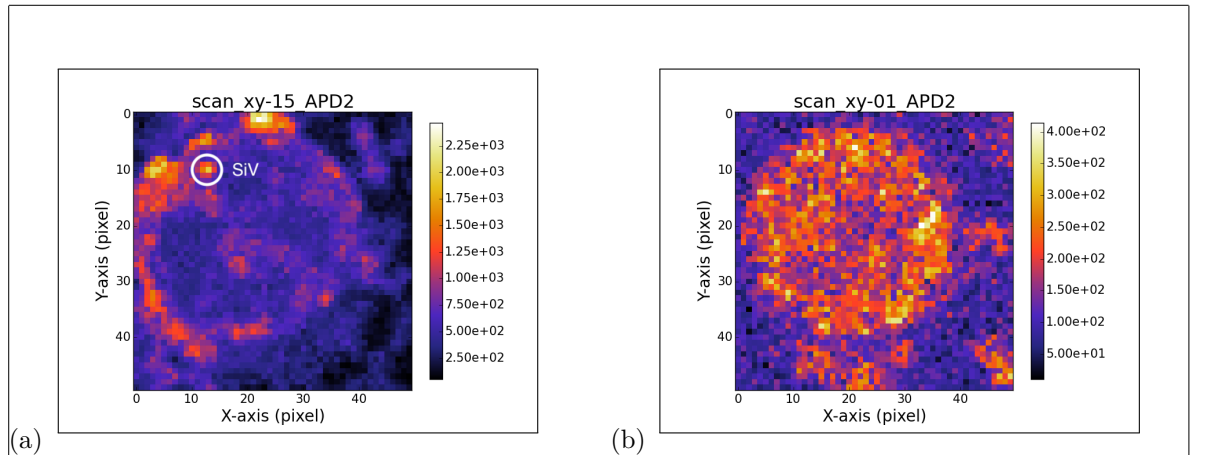


Figure 1.10: (a) Scan of the VCSEL Bm4 with coupled nanodiamond under excitation with the laser from the confocal setup. The big visible ring is the edge of the circular aperture in the *p*-contact of VCSEL Bm4. The bright spot in the upper left corner corresponds to the transferred nanodiamond containing an SiV center causing a spike in the countrate. (b) Scan of the VCSEL Bm2 lacking a nanodiamond under excitation with the laser from the confocal setup. The circular aperture in the *p*-contact exhibits a constant countrate. Note the different scales.

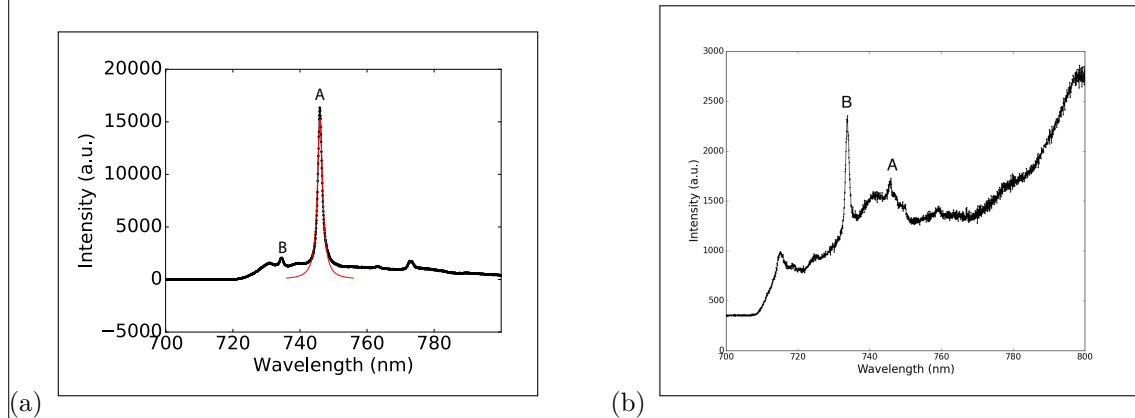


Figure 1.11: (a) Spectrum of the preselected diamond for transfer onto VCSEL Bm4 before pick-and-place. The strong line denoted *A* exhibits a center wavelength of 746.0 nm and a linewidth of 1.9 nm. Line *B* exhibits a center wavelength of 0 nm and a linewidth of 0 nm
 put in correct numbers

(b) Spectrum of the same SiV center after pick-and-place, excited with the same laser as before. While Line *A* is almost gone, line *B* still exists seemingly unchanged and has become the predominant line of the spectrum. We remark that due to material restrictions, different longpass filters were used for the two measurements. Measurement (a) was performed with a 720 nm longpass filter, measurement (b) with a 710 nm longpass filter.

The observed reduction of the intensity of line *A* is difficult to explain. One cause could be damage to the color center due to the electron radiation it was exposed to during the pick-and-place process. This is supported by previous research in this authors group recording reduced fluorescence light intensities after color centers were exposed to electron radiation [?]. However, the fact that line *B* remains virtually the same before and after pick-and-place is curious, raising the question whether damage alone is sufficient to explain the observed effect. As it stands, the question remains open and is thus subject to further investigation.

With line *B* as remaining dominant line we then operated VCSEL Bm4 at 1.84 mA and 3.3 V, turning off the laser of the confocal setup. Thus SiV center exitation is due to the output laser of VCSEL Bm4.

For comparison, we scanned both the surface of VCSEL Bm4 including a nanodiamond as well as VCSEL Bm2 without a nanodiamond. A bandpass filter allowing light between 730 nm to 750 nm to pass was used. This filter window suppresses the VCSEL laser line at 655 nm while leaving the SiV center emission nearly unchanged. The results of the two scans are given in Figure 1.12, where the bright areas correspond to the circular VCSEL output regions. It can be seen that no difference in brightness can be established between a VCSEL with and without a nanodiamond containing a SiV center.

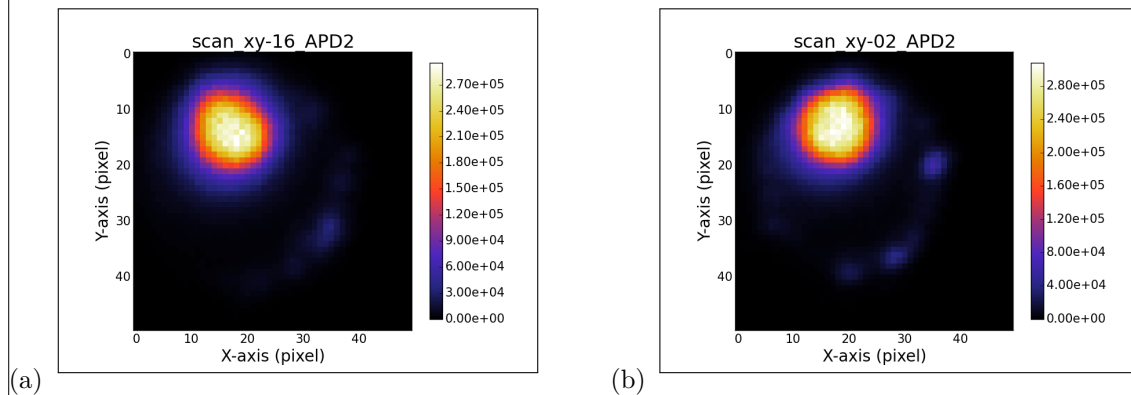


Figure 1.12: (a) Scan of the laser light stemming from VCSEL Bm4 and the fluorescence light from the SiV center in the filter window 730 nm to 750 nm. (b) Scan of the laser light stemming from VCSEL Bm2 without a coupled SiV center. The outcome of the two scans is almost identical.

To further investigate we conduct spectroscopic measurements. Since the position of the nanodiamond in VCSEL Bm4 is known, we measure the spectrum of light originating from this position. A second spectrum is obtained from VCSEL Bm2 measuring the corresponding position without a nanodiamond present. Figure 1.13 reports the results. Again no meaningful difference between the two VCSELs can be established. The lack of any distinct lines in the spectrum taken for VCSEL Bm4 which can be attributed to SiV center emission is striking.

To explain the observation, the following considerations are reasonable: The SiV center is excited by the VCSELs laser and thus emitting single photons which are passing through the filter window. The same is true for photons stemming from VCSEL side band emission. Given that the emission from the side band of VCSEL Bm4 dwarfs the single photon emission of its SiV center, the obtained results are reasonable. To confirm we examine the reflectivity of the DBR of VCSEL Bm4. section 1.14 illustrates that the DBR exhibits imperfect reflexivity

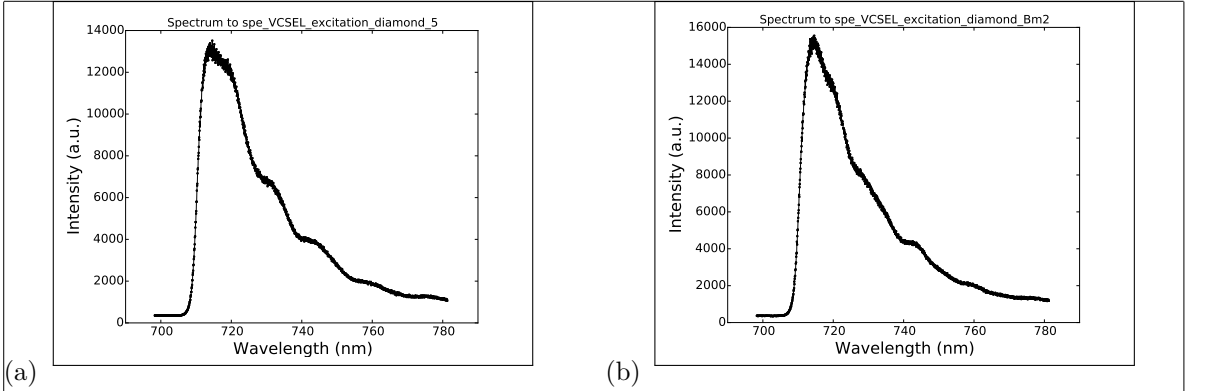


Figure 1.13: (a) Recorded Spectrum of the SiV center in the transferred nanodiamond coupled to VCSEL Bm4 during VCSEL operation. No distinct SiV center lines are visible. (b) Recorded spectrum of VCSEL Bm2.

in the wavelength region relevant for SiV center emission. As a result, relevant side band emissions of VCSEL Bm4 are not sufficiently suppressed to allow for SiV center emission to be detected. This in turn means that our initial attempt to realize a hybrid-integrated single photon source by coupling an SiV center to a VCSELs is thwarted by large side band emissions of the latter.

Despite a failed first attempt, a clear direction for further improvement was identified, i.e. focusing on ways to reduce VCSEL side band emission in the relevant SiV center emission regime. A promising approach to suppress the side band is to add a gold layer on top of the VCSEL acting as an additional mirror. While films of gold have a transmittance maximum at 500 nm, the transmittance minimum depends on the film's thickness [?]. Thus a gold layer could in principle be used to suppress the VCSEL side band in the SiV center emission regime. Provided such a layer can be engineered and is effective, one may expect SiV center emission to be recovered. Efforts in this direction are a required next step towards the realization of hybrid-integrated single photon sources based on SiV centers coupled to VCSELs.

1.3 Coupling Nanodiamonds to Double Bowtie Antenna Structures

In this chapter, the integration of SiV centers in nanodiamonds with double bowtie nanoantenna structures is presented. The emission from the coupled system has two advantages:

- The antenna causes an enhancement in the SiV center's photoluminescence emission intensity.
- The photoluminescence spectrum of the nanodiamond is modified depending on the geometry of the nanoantenna as well as the position of the emitter in the gap. This provides the flexibility of designing the nanoantennas to accurately predict and tune the emitters' PL spectrum as desired.

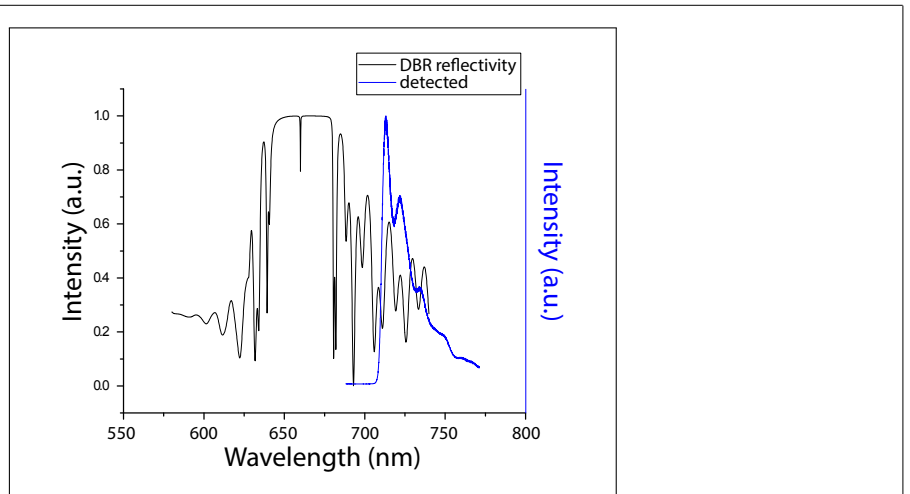


Figure 1.14: Reflectivity of the Distributed Bragg reflector (DBR) of VCSEL Bm4 [?], and a spectrum of the SiV center measured during VCSEL excitation for comparison. The reflectivity of the DBR and the VCSEL emission spectra are depicted with different scales. The shape of the measurement of the SiV center during VCSEL operation is reminiscent of the shape of the DBR reflectivity. The spectrum of the SiV center is not visible. As the emission from the SiV center is small compared to the intensity of the laser side band in the same wavelength regime, the SiV centers emission is not detectable

warum schaut das spectrum anders aus als das, was einzeln geplottet ist?

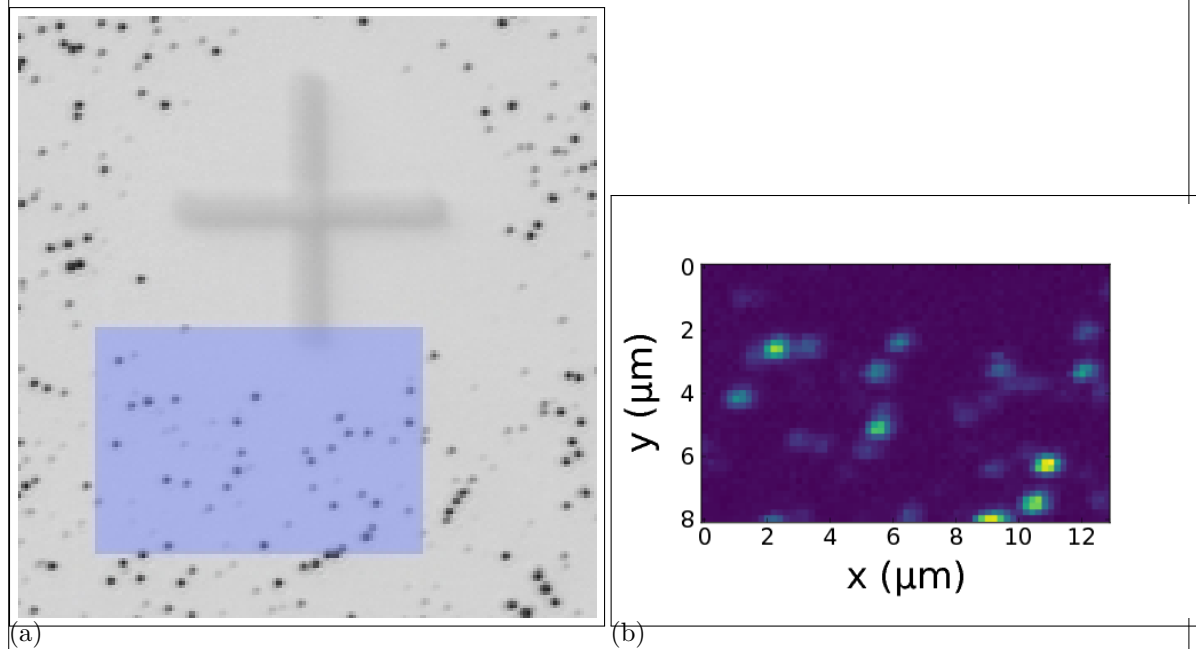


Figure 1.15: (a) Picture recorded with a commercial high resolution laser scanning microscope. The area shaded in blue represents the photoluminescence scan in image (b). (b) Photoluminescence scan of a $8 \mu\text{m} \times 13 \mu\text{m}$

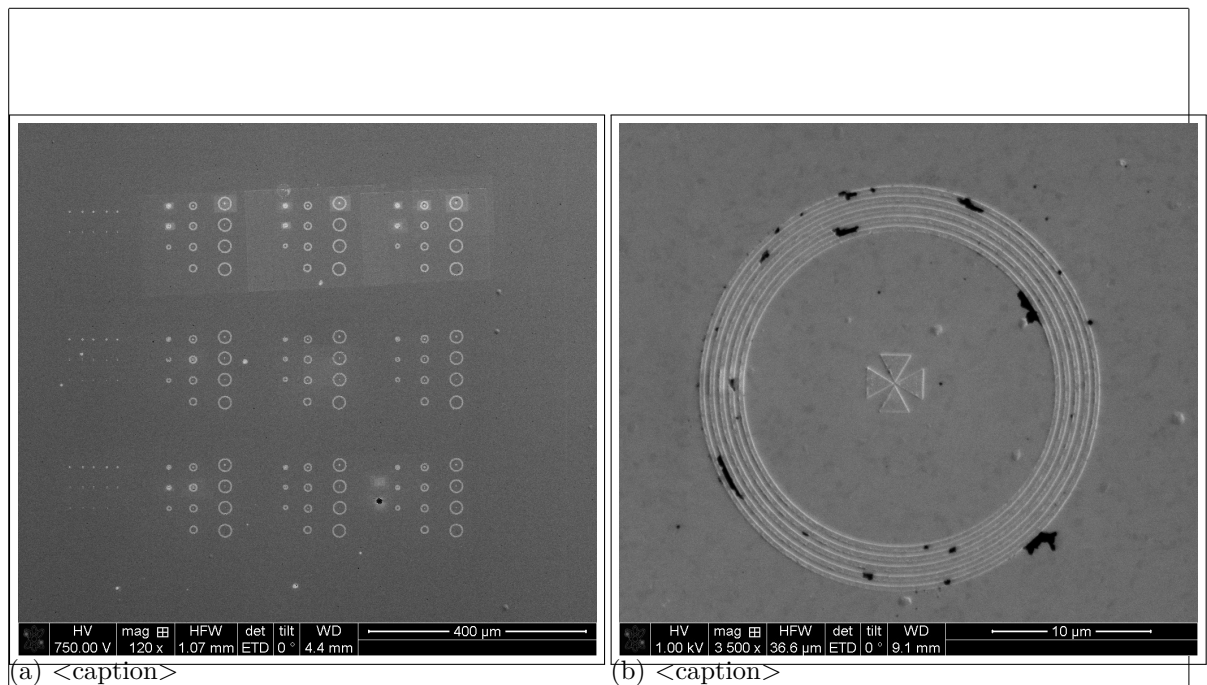


Figure 1.16: <caption>

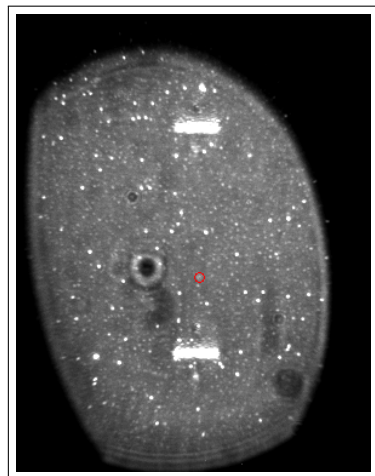


Figure 1.17: Image of the sample surface of 100 nm wet-milled nanodiamonds spin-coated on an iridium substrate illuminated with diffuse white light. The white bars are the horizontal bars of the cross markers which serve as a coarse orientation on the sample surface, the white dots are nanodiamonds, the big black spot is an artifact.

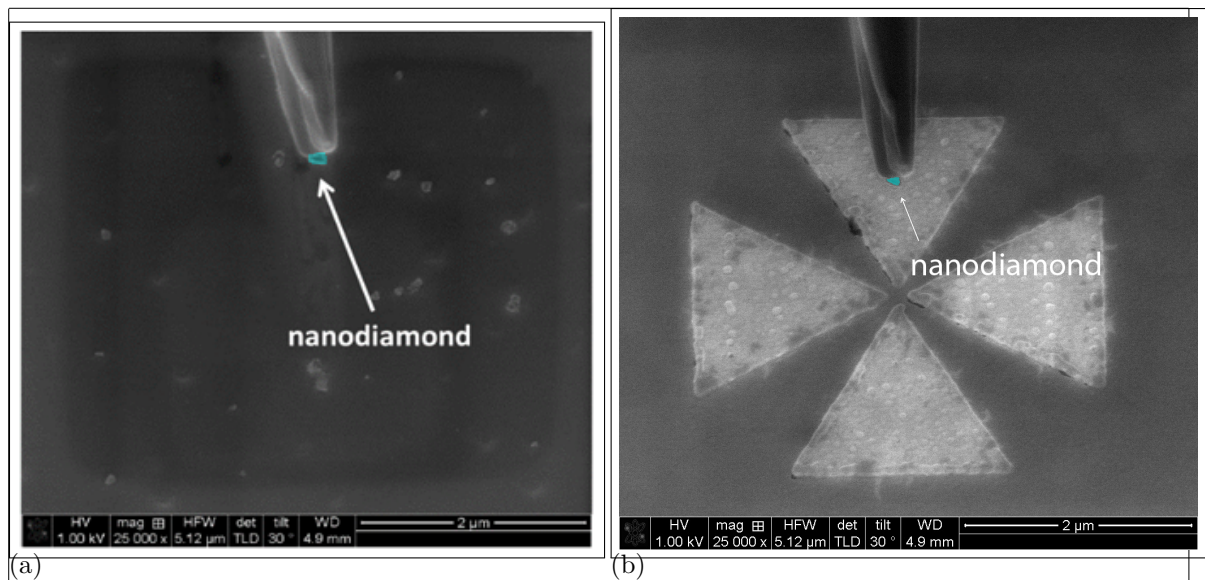


Figure 1.18

1.3.1 Plasmonic Antennas

[?] Optical antennas, acting as converters between propagating and localized fields, provide an effective route to couple photons in and out of nanoscale objects. These antennas are the counterparts of conventional radio and microwave antennas and operate in the visible regime (1, 2). Optical antennas have been shown to focus optical fields to subdiffraction-limited volumes (3), enhance the excitation and emission of quantum emitters (4 \AA), and modify their spectra (8).

A characteristic of antennas is their directed emission and reception. So far, the control of directionality has mainly been pursued by photonic crystal structures (9) and surface-plasmon-based devices (10–12). However, for such structures approaching the nanometer scale diffraction can limit the collimated beaming of light. On the other hand, the interaction of quantum emitters with light is best enhanced with microcavities (13, 14). Compared with these approaches, plasmonic nanoantennas offer a much smaller footprint in an open geometry combining strong subwavelength fields and increased transition rates, together with the prospect of directionality.

[?] from gold, a metal that can develop charge oscillations in its surface layers when excited by optical radiation. These antennas allow visible radiation, which has wavelengths of hundreds of nanometers, to couple into a semiconductor quantum dot only a few nanometers in diameter, and also direct the emission.

Good mode-matched antennas reradiate their energy after excitation within a single cycle of the wave. Molecules or quantum dots take nanoseconds or even longer to reradiate their energy. This time scale corresponds to about 1 million oscillations at optical frequencies, and the emission is in all directions.

If an atom, molecule, or quantum dot is placed into the near-field of a metallic nanoantenna (within about 1/50th the wavelength of the emitted radiation), its excited state can radiate photons very efficiently to free space (see the figure, panel B). The quantum emitters can emit a single photon, which can be exploited in quantum optics. Additionally, the

nanoantenna can redirect radiation into a defined solid angle in space and impose a specific polarization on it.

The demonstration of the Purcell effect, which is the acceleration of the decay of the quantum emitter caused by impedance matching by the antenna to free space, could also enhance the radiative emission over nonradiative losses

[?] The electro-magnetic antenna, originally referred to as an "aerial", is a transducer between electromagnetic waves and electric currents, and generally operates in the radiofrequency regime. In analogy with the electro-magnetic antenna, we define the optical antenna as a device that converts freely propagating optical radiation into localized energy, and vice versa. The spatial extent of a receiver or transducer is commonly much smaller than the wavelength of radiation, λ , and is typically of the order of $\lambda/100$.

Surface plasmon resonances make optical antennas particularly efficient at selected frequencies. A generic antenna problem is illustrated in Fig. 3. It consists of a transmitter and a receiver, both represented by dipoles p . The antenna is introduced to enhance the transmission efficiency from the transmitter to the receiver. This enhancement can be achieved by increasing the total amount of radiation released by the transmitter, for which the antenna efficiency is a useful figure of merit:

$$\eta = \frac{P_{rad}}{P} \quad (1.1)$$

where P is the total power dissipated by the antenna, P_{rad} is the radiated power and P_{loss} is the power dissipated through other means, such as by absorption in the antenna. However, the transmission efficiency can also be improved by directing the radiation in the direction of the receiver. The efficiency for this process is represented by the directivity:

$$\eta = D \quad (1.2)$$

where the angles $\hat{\theta}$ and $\hat{\phi}$ represent the direction of observation and $D(\hat{\theta}, \hat{\phi})$ is the angular power density. The combination of antenna efficiency and directivity is referred to as the antenna gain:

$$G = \eta D \quad (1.3)$$

By reciprocity, we can interchange the fields and sources in Fig. 3 to give $G = \eta D$, where E_1 (E_2) is the field of dipole p_1 (p_2) evaluated at the location of p_2 (p_1). A good transmitting antenna is therefore also a good receiving antenna. For a transmitter in the form of a two-state quantum emitter, reciprocity leads to a relationship between the emitter's excitation rate \dot{N}_{exc} and its spontaneous emission rate:

$$\eta = \frac{\dot{N}_{exc}}{\dot{N}_s} \quad (1.4)$$

Here, the superscript "0" refers to the absence of the antenna and the subscript "1" indicates the polarization state; that is, the electric field vector points in the direction of the $\hat{\theta}$ unit vector. An equivalent equation holds for polarization in the $\hat{\phi}$ direction. Interestingly, excitation in a direction of high directivity allows the excitation rate to be enhanced more strongly than the radiative rate. Another important antenna parameter is the antenna aperture, which is formally the same as the absorption cross-section sigma. Let us consider a dipole-like receiver with a cross-section σ that is not coupled to an antenna. The unit vector in the direction of the absorption dipole axis is denoted as n_p and the incident field at the location of the receiver is E_0 . Once we couple the receiver to an antenna, the field at the receiver increases to E and the cross-section or antenna aperture becomes

$$\eta = \frac{\sigma}{\sigma_0} \quad (1.5)$$

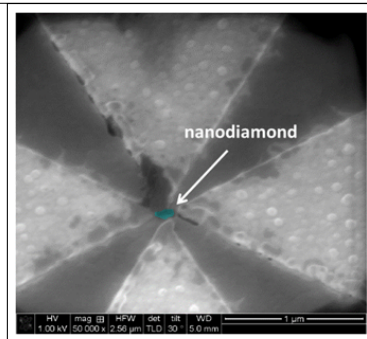


Figure 1.19: <caption>

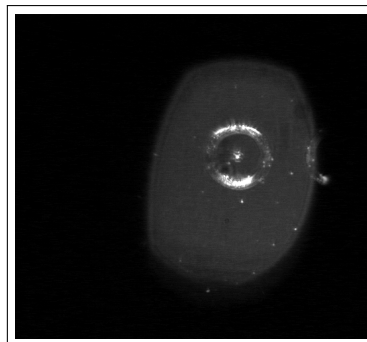


Figure 1.20

Thus, the aperture of an optical antenna scales with the local intensity enhancement factor. Theoretical and experimental studies have shown that intensity enhancements of 10^4 – 10^6 are readily achievable^{14,36,37} and hence, for typical molecules with π -free-space cross-sections of $\sigma_{\text{mole}} = 1 \text{ nm}^2$, we find that a layer of molecules spaced $0.1\text{--}1 \text{ nm}$ apart can absorb all of the incident radiation if each molecule is coupled to an optical antenna. Of course, this estimate ignores the coupling between antennas and therefore has limited validity.

1.3.2 Structure of the Plasmonic Antennas

FDTD numerical simulations were performed using Lumerical software to characterize gold double bowtie nanoantennas on a gold substrate. The nanoantennas are tailored to have a gap of $g = 150 \text{ nm}$ (taking into account the diameter of the nanodiamonds of around 100 nm), side length of $L = 2 \mu\text{m}$, and a thickness of $t = 60 \text{ nm}$ (see Fig. 3a). Upon excitation with incident light, an intense electromagnetic hotspot is formed in the nanoantenna gap [?], which is expected to excite a nanodiamond containing SIV centers aiming to enhance its fluorescence emission. Unlike a single bowtie that is sensitive only to the polarization along its principle axis (C₂ rotational symmetry), a double bowtie features a C₄ rotational symmetry and therefore focuses both parallel and perpendicular polarizations (i.e. all in-plane directions). The index of refraction of gold is taken from Palik [], and that of the nanodiamond is chosen to be $n = 2.4$ at $\lambda = 660 \text{ nm}$. The electric field intensity in the nanoantenna gap is then measured as a function of wavelength to identify the antenna resonance. The spectrum is given in Fig. 3b where we observe that the resonance shows two peaks; an intense peak coinciding with the

read paper

Palik, E. D. Handbook of optical constants of solids. 3, (Academic press, 1998)

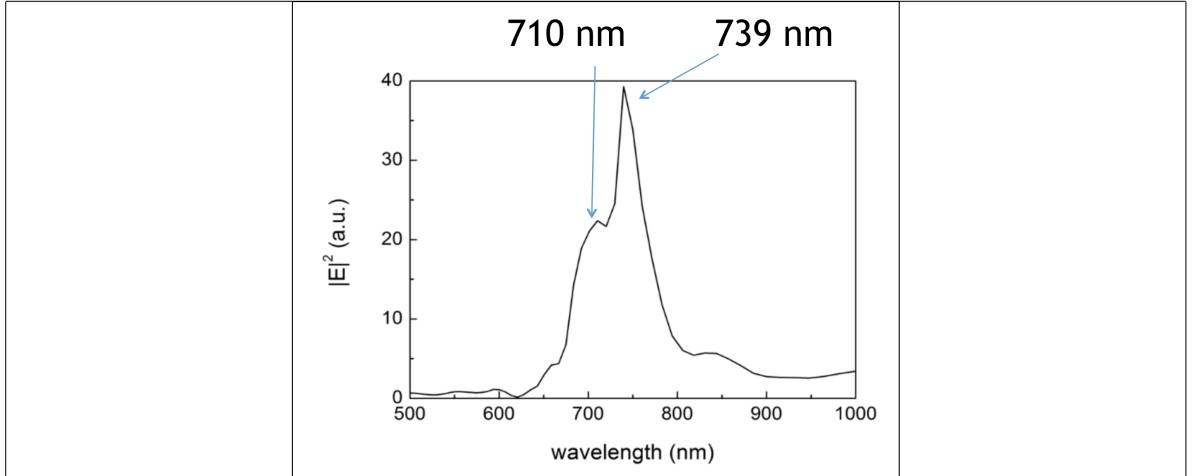


Figure 1.21: <caption>

SiV emission wavelength ($\lambda = 739 \text{ nm}$), and an additional mode at a lower wavelength ($\lambda = 710 \text{ nm}$) [?]. The resonance spectrum of the antenna alone shows only one peak at 739 nm. Thus, the additional peak is attributed to the presence of the nanodiamond that is slightly shifted from the center of the gap, corresponding to our experimental conditions. These calculations suggest, that the emission from an SiV center at 738 nm is effectively enhanced and directed by the antenna.

1.3.3 SiV center in a Plasmonic Double Bowtie Antenna

In the following, specific details and challenges concerning the coupling process are given and results of the spectroscopic measurements of an SiV center in a plasmonic double bowtie antenna are reported.

We performed coupling the nanodiamonds containing SiV centers in two approaches: First we chose a nanodiamond containing several SiV centers for pick-and-place and afterwards a nanodiamond containing a single SiV center. As mentioned before, single SiV centers may be damaged by the electron radiation in the SEM during pick-and-place and stop emitting photoluminescence light. Hence, we decided to run first experiments with nanodiamonds containing multiple SiV centers. This approach has the advantages that we are able to gain experience in the execution of the pick-and-place process without the risk of permanently damaging the emitter and therefore rendering the tedious pick-and-place process futile. For measurements of the intensity enhancement by the antenna, a single emitter is necessary. However, the antenna's influence on the SiV center spectrum can be studied when several emitters are present. Therefore, studies of the spectrum are performed in this first approach.

After we gained experience with the first approach, we searched for a suited nanodiamond containing a single SiV center. The aim was to perform saturation and second order correlation measurements to probe single SiV centers, and consequently quantify the exact Purcell enhancement imposed by the nanoantenna on a single photon emitter.

Nanodiamond With Multiple SiV centers Coupled to Antenna

The nanodiamonds exploited for the approach of coupling multiple SiV centers to an antenna were produced by a wet-milling process from a CVD diamond film¹. The solution of nanodiamonds which exhibit a median size of 100 nm were spin-coated on an iridium substrate treated with Piranha etch. To ensure that a pre-characterized nanodiamond exhibiting preferred optical properties (eg. narrow linewidth, high count rate) is later found again, the iridium substrate was engraved with reference cross markers produced by a focused ion beam prior to the spin-coating process. After spin-coating, the sample was placed in an oven for 3 hours at 450 °C to oxidize the surface and remove any residual graphite and amorphous carbon.

?? shows the spectrum recorded of the preselected nanodiamond. The ZPL peak exhibits a wavelength of 738.55(1) nm and a linewidth of 5.00(3) nm. These numbers correspond well to the ZPL of unstrained SiV centers and therefore allows us to deduce that the studied nanodiamond contains at least one SiV center. Photon autocorrelation measurements revealed, that the nanodiamond contains multiple SiV centers.

To determine the position of the nanodiamond on the original substrate, first a scan with a commercial laser scanning microscope (LSM) was performed as described in ?? . ?? shows a part of an obtained LSM image. The cross marker can easily be identified, the black dots are nanodiamonds. After transferring the sample into the confocal setup, confocal scans of the corresponding areas are performed (??). The area corresponding to the fluorescence light scan in ?? is shaded blue in ?? . When looking closely, the bright spots in the fluorescence light scan can be identified with nanodiamonds visible in ?? . The image in the SEM is very similar to the image obtained by the LSM. Therefore, once a nanodiamond containing a preselected emitter is identified in the LSM scan, it is easy to find the same emitter in the SEM.

The picking part of the pick-and-place process was performed in the same manner as described in the section about VCSELs (??). The gold surface of the plasmonic antenna caused a high adhesion between the antenna surface and the nanodiamond. Once the nanodiamond touched the gold, it could not be picked up again with the tungsten tip. The nanodiamond first touched the antenna structure a few nanometers away from the gap and immediately stucked to the surface, on top of one of the triangles. Therefore, the nanodiamond had to be pushed into the gap with the nanomanipulator tip. This process caused some damage to the antenna structure. The damage is visible as black area at the tip of the top triangle in ?? . However, FDTD simulations of damaged antennas reveal that this modification of the antenna hardly influences the antenna resonance.

After this deterministic placement we measure the PL spectrum of the nanodiamond to identify the effect of the nanoantenna on its emission. The result is displayed in ?? . The additional peak at a lower wavelength is attributed to the antenna resonance mode. To verify this, we convolute the experimental PL spectrum of the nanodiamond measured before placing it in the nanoantenna (??) with the intensity spectrum of the nanoantenna obtained by simulations (??). The resulting spectrum is given in ?? , and is in good agreement with the measured spectrum in ?? , confirming that indeed the extra peak is due to the antenna resonance.

¹wet-milling performed by A. Muzha, group of A. Krueger, Julius-Maximilians Universität Würzburg, diamond film grown by group of O. Williams, School of Engineering, Cardiff University

fehlergrenzen
verfünen
machen

bild dazu

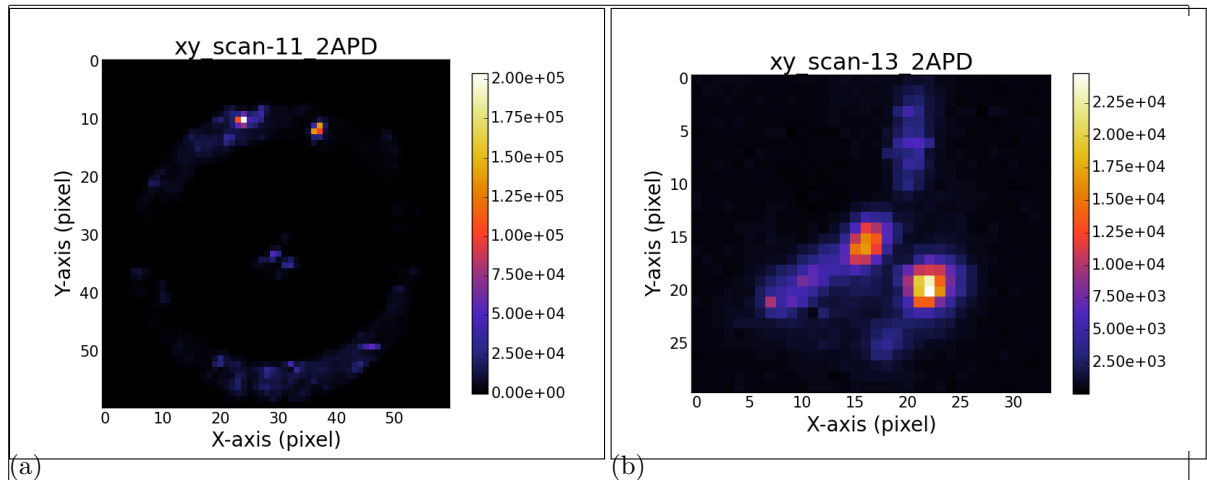


Figure 1.22: <caption>

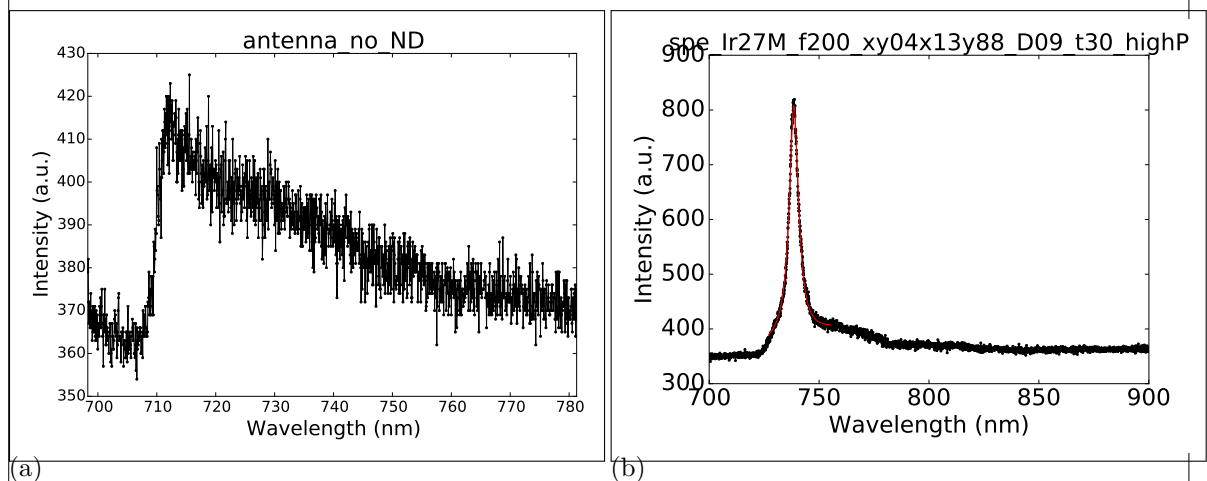


Figure 1.23: <caption>

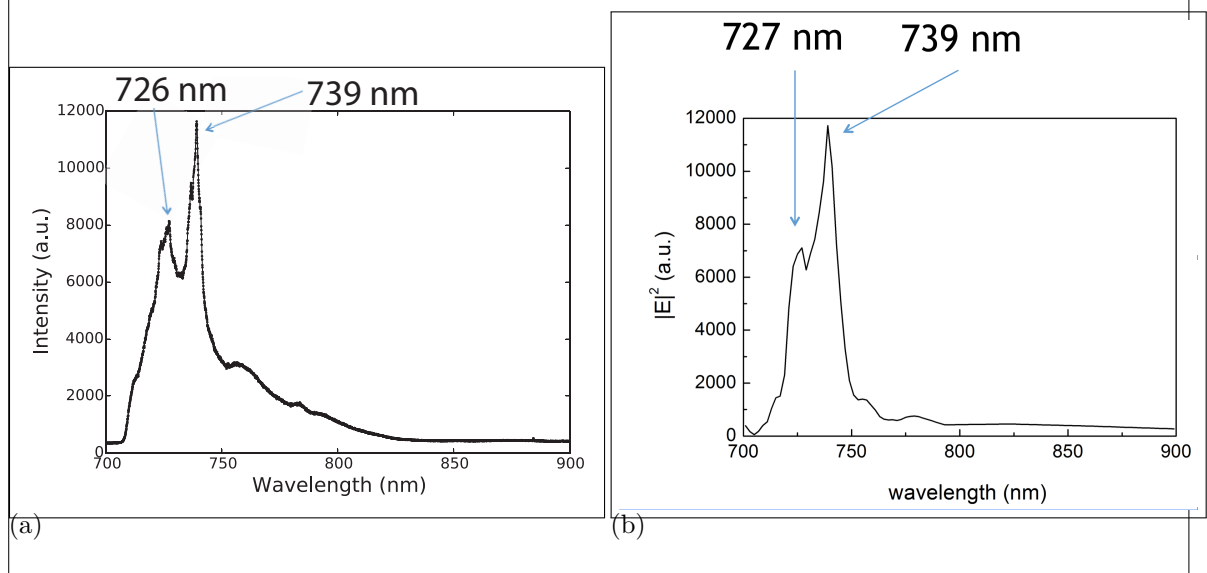


Figure 1.24: <caption>

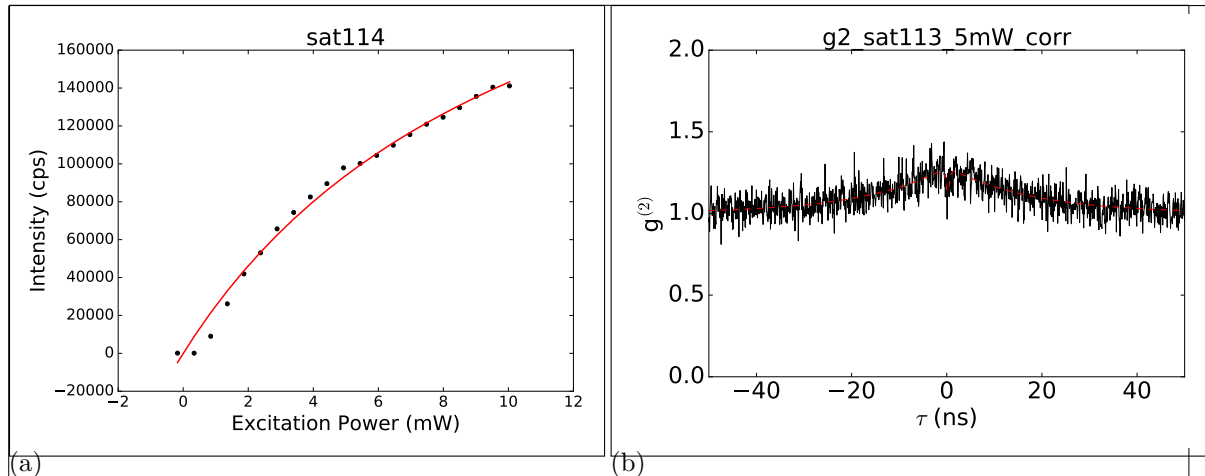


Figure 1.25: <caption>

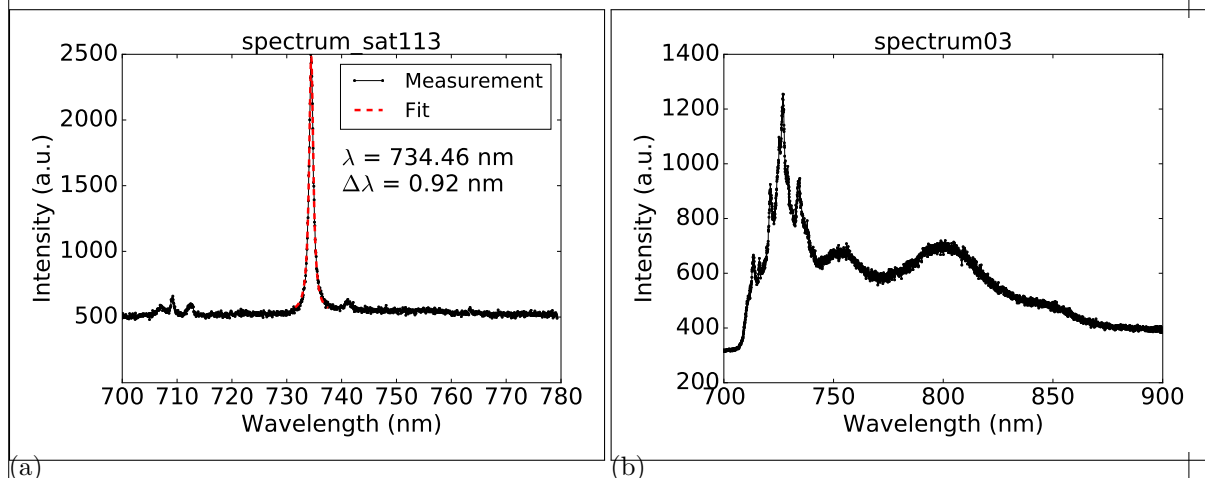


Figure 1.26: <caption>

Nanodiamond With Single SiV center Coupled to Antenna

sample M02-16: drop-casted with SiGH45 First, only a small percentage of the technically suited nanodiamonds (size, isolation) contain a single SiV center, second, damage due to electron radiation during pick-and-place. After an SiV center with a small dip in the $g^{(2)}$ function, indicating only few SiV centers.

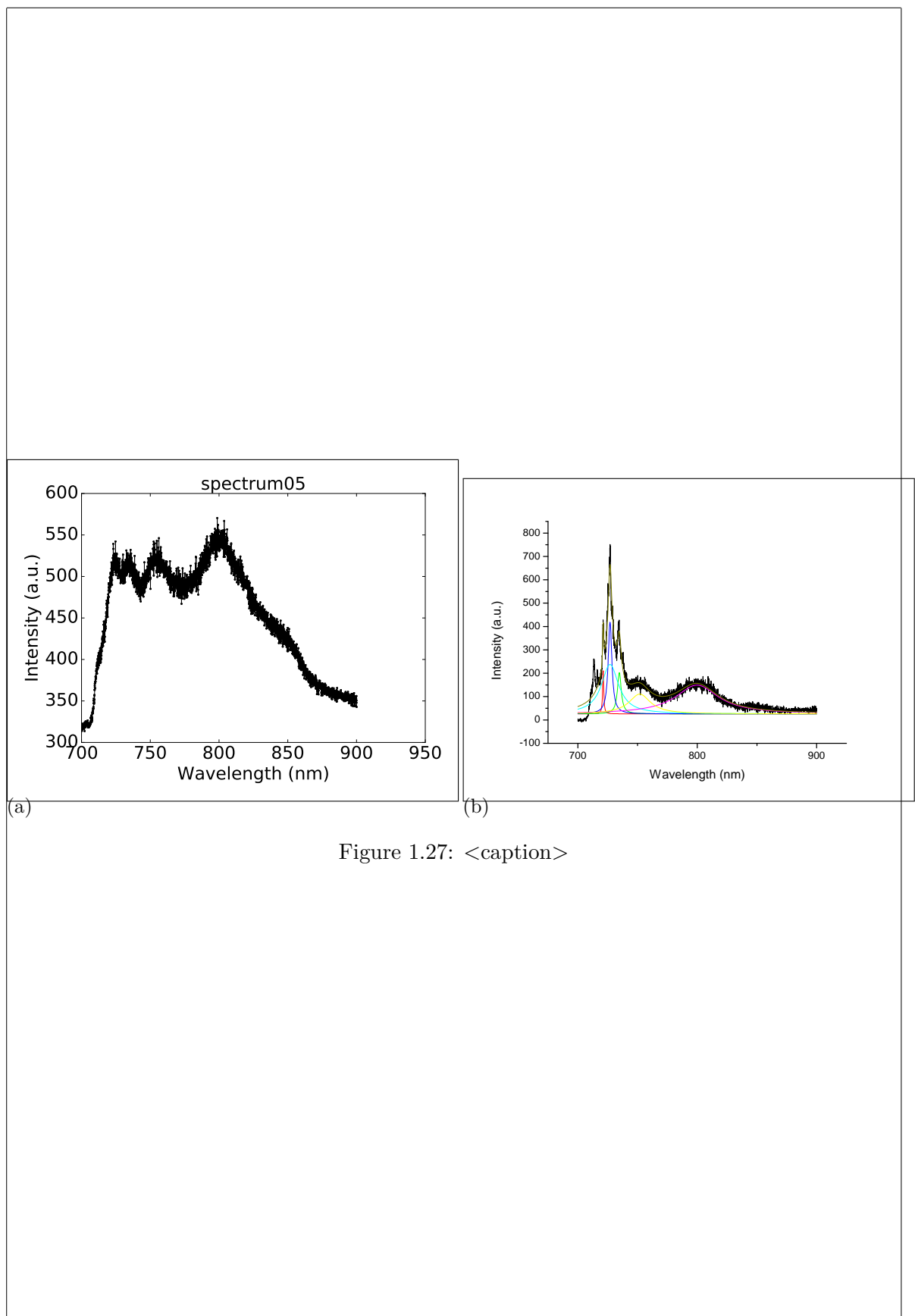


Figure 1.27: <caption>